Use of twenty years CLUSTER/FGM data to observe the mean behavior of the magnetic field and current density of Earth's magnetosphere

Patrick Jean-François Robert[1] and Malcolm W Dunlop[2]

[1]LPP/CNRS Ecole Polytechnique
[2]Beihang University

November 23, 2022

Abstract

The data from the CLUSTER FGM magnetometer, recorded for 20 years at ESA's Cluster Science Archive, have been used to form a database aligned in time. It allows the calculation of curl(B) over all the life of the mission. The B and J data are then averaged, as a function of the dipole tilt angle, to form a 3D grid of spatial extend of 20 RE, and for any spatial resolution. From these data grids, maps of the direction of the magnetic field and of the current density are produced, allowing the observation of the average behavior of the magnetic field and the current density on a large scale. The validity of the calculation of J is discussed. By means of spatial interpolation, the grids are used to provide a measurement of the magnetic field at any point in space where the grid is filled. This allows possibility of ray tracing to obtain empirical plots of the magnetic field lines, i.e. not theoreti-cal, but from experimental data. Field lines near the cusp are visualized, even if they are very smoothed by the averaging of IMF and solar wind parameters. In a future work it would be possible to add other classification than just the dipole tilt angle, such as various activity indicese and solar wind parameters. The prospect of adding data from other missions would extend the regions that have been covered by Cluster, and in-crease the spatial extent of the 3D grid and its resolution.

Use of twenty years CLUSTER/FGM data to observe the mean behavior of the magnetic field and current density of Earth's magnetosphere

P. Robert[1] and M. Dunlop[2,3]

[1]Laboratoire de Physique des Plasmas,CNRS, École polytechnique, Palaiseau, France.
[2]School of Space and Environment, Beihang University,100191, Beijing, China.
[3]RAL, Chilton, Oxfordshire, OX11 0QX, UK.

Key Points:

- Twenty years of data from the CLUSTER / FGM magnetometer allowing the calculation of curl(B) over the entire duration of the mission, have been used to constitute a database aligned in time.
- The compilation of all data leads to the construction of a 3-D grid containing experimental averaged values, while spatial interpolation makes possible the computation of magnetic field lines.
- A rough average of cusps positions and shape, according to values of dipole tilt angle, can be determined thanks to field line tracing.

Corresponding author: Patrick Robert, `patrick.robert@lpp.polytechnique.fr`

Abstract

The data from the CLUSTER FGM magnetometer, recorded for 20 years at ESA's Cluster Science Archive, as well as the position of the spacecraft, have been used to form a database aligned in time. It allows the calculation of curl(B) over all the life time of the mission (representing the current density via $\mu_0\vec{J} = c\vec{url}\vec{B}$). The $\vec{B}$ and $\vec{J}$ data are then bin averaged, as a function of the dipole tilt angle, to form a 3D grid of spatial extent of about 20 R_E, and for any spatial resolution. From these data grids, maps of the direction of the magnetic field and of the current density can be produced, allowing the observation of the average behavior of the magnetic field and the current density on a large scale.

The validity of the calculation of $\vec{J}$ is discussed. By means of spatial interpolation, the grids are used to provide a measurement of the magnetic field at any point in space where the grid is filled. This allows yhe possibility of ray tracing to obtain empirical plots of the magnetic field lines, i.e. modelled from experimental data. Field lines near the cusp can be visualized, although smoothed by the averaging of the IMF and solar wind parameters. In future work it would be possible to add other classification criteria than just the dipole tilt angle, such as various activity indicese and solar wind parameters.The prospect of adding data from other missions (such as MMS) would extend the regions that have been covered by Cluster, and in-crease the spatial extent of the 3D grid and its resolution.

1 Introduction

The four CLUSTER S/C have continuously provided excellent data for twenty years, and these data are carefully archived regularly at the Cluster Science Archive (CSA) of ESA (Laakso et al., 2010). This huge database contains, among other things, the data from the FGM magnetometer (Balogh et al., 1993, 1997; Dunlop et al., 2002). These data are used here to observe the average behavior of the magnetic field around the Earth, notably inside the magnetosphere.

In the GSM frame, the form of the mean magnetic field is driven mainly by the value of the dipole tilt angle. The values of the field can be distributed in spatial grids, dependent on this angle. For the purpose here we also do not separate any dependence on either geomagnetic or external conditions (solar wind and interplanetary magnetic field). This can be explored in principle with the database in future work. To do this, we make spatial average in each cell of the grid, and then obtain temporal averages over the twenty years of measurements. Of course, this proceedure erases transient effects on short temporal scales, but we obtain the value of the averaged experimental field in an extended spatial volume, which is not without interest. As CLUSTER allows access to spatial gradients, giving quantities such as curl(B) and div(B), we calculate the linear approximation to these quantities for all the available values of B, and we set up a large database of curl(B) and div(B) covering the same twenty years. Average 3-D grids of these quantities can be calculated , and the production of various maps of averaged $\vec{J}$ in magnitude and direction, allows us to observe the global behaviour of the currents.

2 Data Access and Processing

All FGM data used in this paper were downloaded from the CSA (Laakso et al., 2010) in CEF format (Allen et al., 2004), as well as all satellite position data. The FGM data used are those having "spin resolution", at around 4 seconds. Over the 19 years taken into account, 27 794 cef files have been downloaded for a total size of 45.5 GB. In order to be able to process them more efficiently these files are converted in binary format, without header and containing both magnetic field and positions. This base will be called hereafter *'FGM_POS_database'*. Its size is 28.4 GB.

To calculate rotational and divergence, it is necessary to have the 4 measurements of $\vec{B_{ij}}$ and the 4 positions $\vec{P_{ij}}$ measured on the same timeline (i=1,3 j=1,4). It is therefore necessary to interpolate the values of the field, and to bring them back to the same common time, then to interpolate the spacecraf positions to have these values at the same times as the magnetic field. So we have established a *'spin resolution time-aligned database'* with the same time stamp for the 4 satellites, in field and in position, and this is for 19 years of data (2001-2019 included). This base, whose size is $\sim$ 28 GB, will be called hereafter *'FGM_POS_aligned_database'*. The 20^{th} year of data can be added when available from the CSA.

Figurez 1 displays the cumulative point count of each cell in a high resolution data grid (0.25 R_E), in XY, XZ and YZ planes. Total number of tetrahedra is $\sim$ 150 million into the cube, i.e. 600 million of measured $\vec{B}$ vectors. Superimposed on these maps, the bow shock is plotted (Rodriguez-Canabal et al., 1993). The limit of the closed field lines, computed as described in a later section 5.1, is also drawn as a simple geometric indication. It is not exactly the magnetopause, but gives a rough approximation of it, and is no time-dependant as the averaged data.

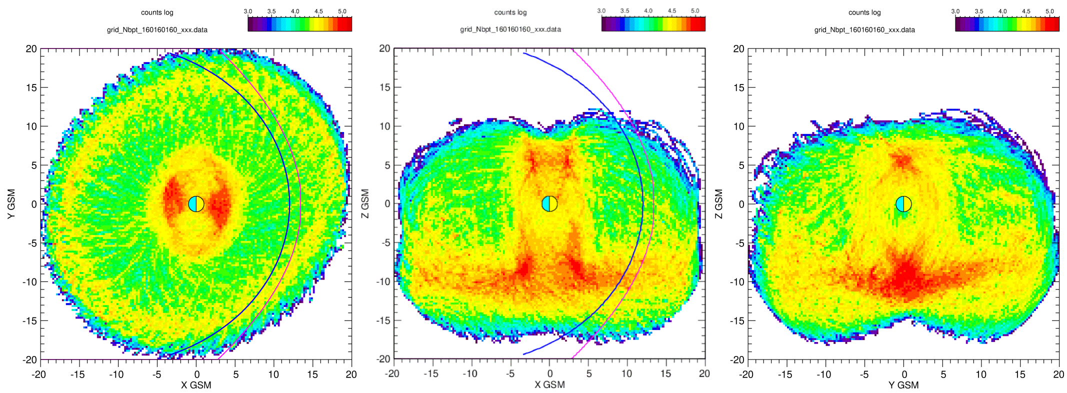

Figure 1. Cumulative number of points in a hight resolution data grid (0.25 R_E), in XY, XZ and YZ planes (log scale).

3 Observation of Averaged Magnetic Field

From the binary *FGM_POS_database*, we computed the averaged magnetic field in a 3D grid of 0.25 R_E spatial resolution, for various dipole tilt angles θ. The magnitude of the field is shown in a planar cut such as meridian or equatorial plane thanks to a color code. As previously the bow shock is plotted, as well as the limit of the closed field lines.

As an example of the database output figure 2 shows the magnitude of the DC field in the meridian plane (top), for $\theta = -10$ (winter in Northern hemisphere) and $\theta = +10$ (summer in Northern hemisphere). The magnitude decreases like a dipole, with a sudden drop beyond the bow shock, and the magnitude in the tail is weak, as expected. Bottom of figure 2 shows the same output but in the equatorial plane. Note that in the equatorial plane the dawn side is observed at positif tilt angles and the dusk one at negative.

To plot the direction, we first reduce the spatial resolution of the grid to 0.5 R_E, and the direction is indicated by an arrow in each cell. Figure 3 show the $\vec{B}$ direction in the XZ GSM meridian plane, for $\theta = 0$. We can see a smooth and constant direction in the magnetosphere and a variable one in the magnetosheath and solar wind. We will see later in section 5.2 how use this data grid to draw magnetic field lines.

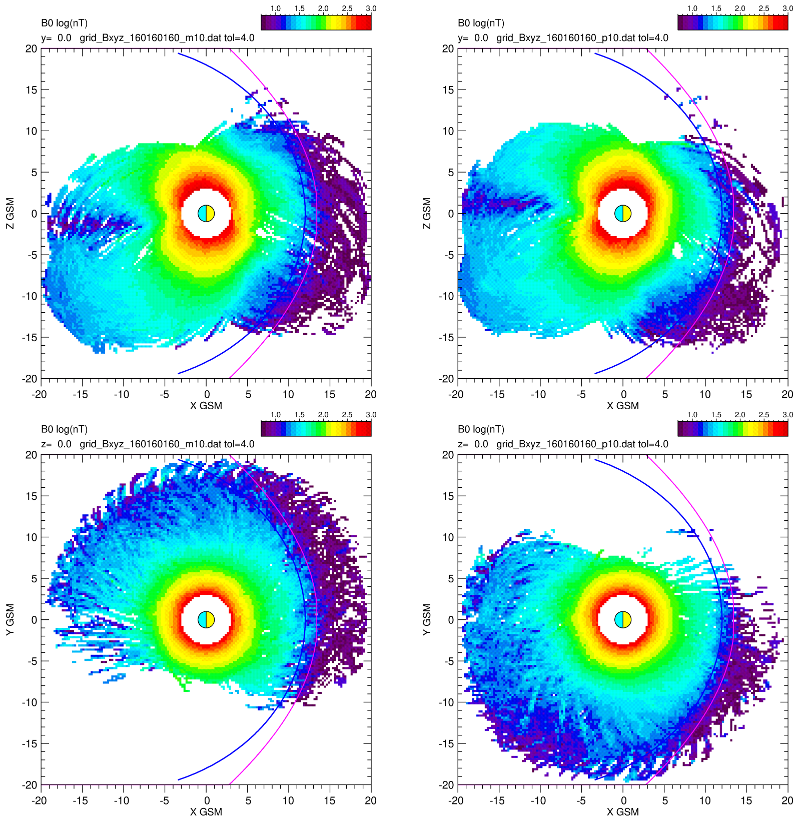

Figure 2. Average of the magnitude of the magnetic field over 20 years in GSM system, for a dipole tilt angle $\theta = -10 \pm 5$ (left) and $\theta = 10 \pm 5$ (right). Top: XZ meridian plane, bottom: XY equatorial plane.

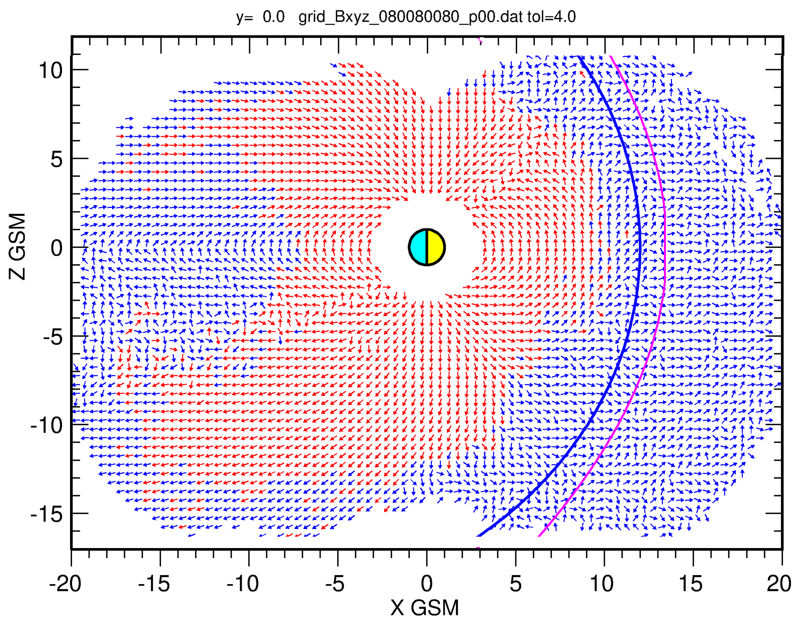

Figure 3. Averaged direction of magnetic field over 20 years in X-Z GSM plane, for $\theta = 0$. In red color: magnitude $> 50nT$, in blue magnitude $< 50nT$.

4 Computation of Current Density

To compute the electric current density, we use the *FGM_POS_aligned_database* of section 2. In this database, we calculated $\vec{\nabla}\times\vec{B}$ and $\vec{\nabla}\cdot\vec{B}$, for each time stamp, without any particular selection of the data for quality (this will be done later). This is carried out for each of $\sim$ 150 million tetrahedra of the database, contained in the 6948 daily files, and results are written in a binary file containing date/time, fields and position of each S/C, curl and div of B, as well as Elongation and Planarity parameters (Robert, Roux, et al., 1998), and dipole tilt angle. This new data base is called *'Curl_Div_database'* and it size is 53.2 GB. Note that we have 3 versions of this database: one from original $\vec{B}$, one with dipole magnetic field subtraction, and one with IGRF magnetic field subtraction.

4.1 Computation Method

The calculation method used for the estimation of curl(B) is that of the classical method of contour integrals on each face of the tetrahedron, by applying Ampere's law on each face:

$$\oint \overrightarrow{B}(M).\overrightarrow{dl} = \mu_0.I$$

By choosing 3 faces out of the 4 possible, and after processing to reduce to an orthonormal coordinate system, we thus can obtain 4 possible values for the estimation of the rotational gradient. In practice, when the tetrahedron is not degenerated, these 4 values are extremely close, and we use as final result the average of these 4 estimations. To compute div(B) we use the divergence law, or Green-Ostrogradski law, as:

$$\iiint_{\mathcal{V}} \overrightarrow{\nabla} \cdot \overrightarrow{B}\, \mathrm{d}V = \oint_{\partial \mathcal{V}} \overrightarrow{B} \cdot \mathrm{d}\overrightarrow{S}$$

This method has been used extensively in all of the many curlometer studies applied to CLUSTER's FGM data. The analysis method to use multipoint magnetometer data appeared a long time before Cluster launch (Dunlop et al., 1988, 1990), as well as the influence of the shape of the tetrahedron on the accuracy of the measurement of currents (Robert & Roux, 1990, 1993; Khurana et al., 1996). Various geometric criteria have been suggested to define the shape of the tetrahedron in relation to the precision of the measurements (Robert, Roux, & Coeur-Joly, 1995; Robert, Roux, & Chanteur, 1995; Robert, Roux, et al., 1998; Robert, Dunlop, et al., 1998; Dunlop et al., 2002; Dunlop & Eastwood, 2008)

Another formulation to compute Curl and Div was developed by G. Chanteur (Chanteur & Mottez, 1993), based on barycentric coordinates. This elegant method estimate the matrix of gradients, the diagonal terms giving the divergence, while the anti-diagonal terms are used to calculate the rotational gradients (Chanteur, 1998) and (Chanteur & Harvey, 1998). To linear order the calculation is identical, but the error handling is slightly different.

4.2 Testing the Method

As we have to make a choice beetween the classical method based on Ampere's law, nicknamed the 'curlometer', and the equivalent barycentric coordinates, we adopt the first method, based on a code developed by the author for over 30 years, and which was used and tested on numerous simulated data. We have to consider three conditions before applying the calculation:

- Eliminate thetrahedra whose shapes are too flat or too long. We know that if the tetrahedron is degenerate, the estimate of div(B) and curl(B) may be false (Robert & Roux, 1990, 1993; Robert, Roux, et al., 1998; Robert, Dunlop, et al., 1998). So, we systematically reject all the estimates of curl and div where the Elongation or Planarity geometric factors of the tetrahedron (Robert, Roux, et al., 1998) are greater than 0.9.

- Limit the size of the tetrahedron: as it is difficult to know if the assumption of linearity is good or not, we can apply a condition based on the size of the tetrahedron, in particular taking the D_{max} inter-spacecraft distance. The choice of the limiting values of D_{max} is the result of a compromise. If we choose a very small value, the result of the linear computation will be reliable, but the measurements errors can become large and we lose a large number of cases, so that the grids bins will be almost empty. Figure 4 show this parameter during the twenty years of the data base. We can see that if we choose a small value, we lose a large part of data. So we choose D_{max} = 10000 km, as a compromise.

- The creation of magnetic residuals by removing the dipole field, and possibly higher moments, are represented by the field given by the IGRF model (Thébault et al., 2015) before applying the calculation (see discussion in Dunlop et al., 2018, 2020) This operation removes the effect of zero current, non linear dipole gradients and is very usefull to improve the quality of the computation as we will see in next section.

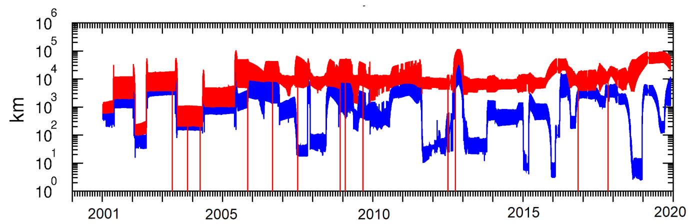

Figure 4. Values of inter distances D_{min} and D_{max} with years

4.3 IGRF field subtraction

In section 4.4 we can compute Curl(B) from individual tetrahedron data ($\vec{B}$ and $\vec{P}$ values at each vertex), but it is also interesting to compute Curl(B) directly from the averaged B grid. For a resolution of 0.25 R_E we define a virtual tetrahedron as follows:

$$P1(i,j,k), \quad P2(i+1,j,k), \quad P3(i,j+1,k), \quad P4(i,j,k+1)$$

The size of the tetrahedron is smaller than the actual tetrahedron, so $\vec{J}$ estimate is better. Furthermore we can use the *FGM_POS_database* rather than the *FGM_POS_aligned_database* which is slightly reduced by the time alignment processing. Figure 5 show the result before and after IGRF field subtraction. Remove the IGRF field before applying the curlometer lead to a more convincing result: The ring current is clearly visible, around 3-8 R_E , with a current density of $\sim 5-20nA/m^2$ corresponding to the previous studies (Zhang et al., 2011). This subtraction decreases the false values near the Earth and makes the ring current more visible. It clearly suppresses the spurious inner currents but leaves the outer signatures largely unaffected. Note that we obtain a closely similar result with the dipole magnetic field subtraction, but a little bit less efficient.

Since we subtracted the IGRF from the measured magnetic field before computation of the current density, it is interesting to see what is the $\vec{B}$ field values wich contribute to the estimate of $\vec{J}$. Figure 6 show this field for the two previous values of θ. This figure can be compared with figure 2 (bottom part) which shows the B field before subtraction of IGRF. All the strong field near the Earth is strongly reduced.

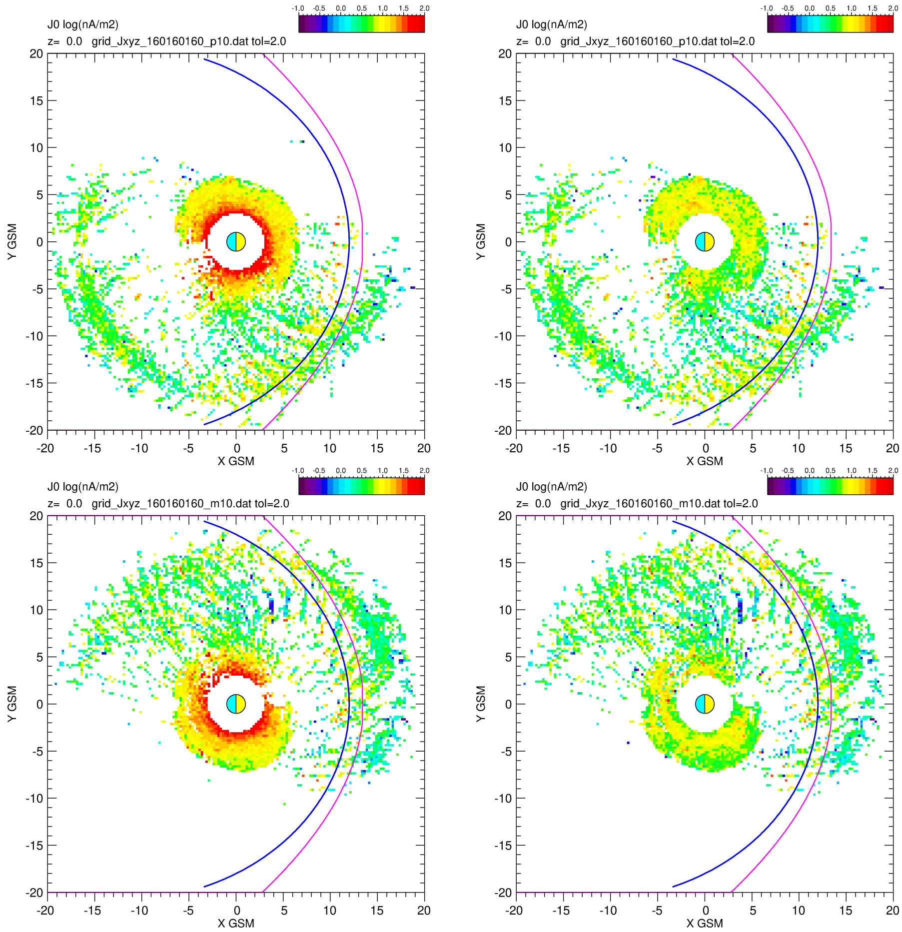

Figure 5. Top: current density from B grid with $\theta = 10$. Bottom: same for $\theta = -10$. Left : result without removing IGRF field before computation. Right: with removing. It can be seen that the anomalous currents are removed to a high degree and globally tend to follow expected large-scale behaviour. Note that the distribution of the data changes with the value of θ, especially in the dawn and dusk regions.

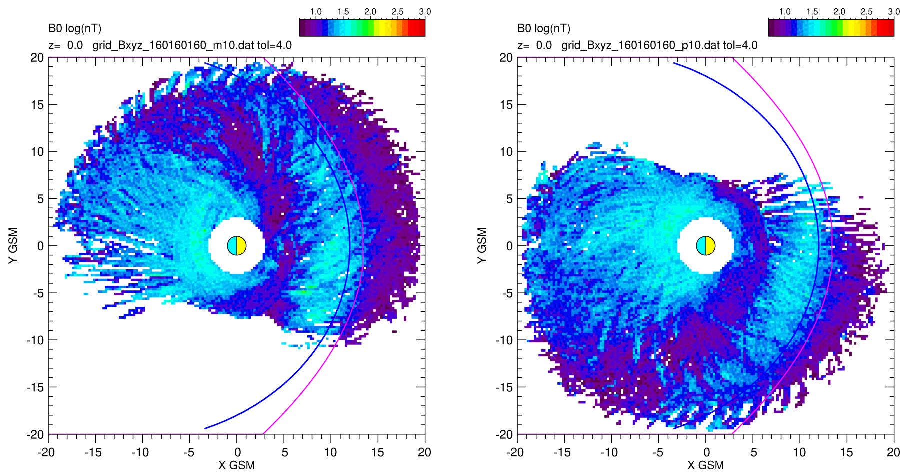

Figure 6. Averaged magnitude of residual magnetic field after IGRF substraction for $\theta = -10$ (left) and $\theta = +10$ (right). To be compared with bottom part of figure 2.

4.4 Observation of Averaged Current Density

In a similar way to the previous $\vec{B}$ processing we now use the classical method to compute $\vec{J}$ from the observed tetrahedron. So we use the *Curl_Div_database* and produce 3D grids containing the averaged values of $\vec{J}$, $|Div(B)|$, $|Div(B)/Curl(B)|$, and the $(\vec{B},\vec{J})$ angle for various dipole tilt angles. Spatial resolution is 0.5 R_E. Computation are done for each tetrahedron of the *'Curl_Div_database'* database with IGRF subtraction. Figure 7 (top) shows the magnitude of the current in the X-Y plane in the GSM system, for $\theta = -10$ (left) and $\theta = +10$ (right). The ring current is clearly visible, around 3-8 R_E, with a current density of $\sim 5-20nA/m^2$. As previously the position and magnitude correspond to expected values (Vallat et al., 2005; Zhang et al., 2011; Yang et al., 2012). The magnetopause current is also visible as red/yellow areas. $|Div(B)/Curl(B)|$ ratio is given on bottom part.

On figure 8 we can see the $(\vec{B},\vec{J})$ angle. In fact, $\vec{B}$ and $\vec{J}$ are perpendicular almost everywhere. The direction of the current density is shown on Figure 9. The direction is roughly clockwise from the Z axe, although for Y > 0 the direction is not clear near the Earth. We can see on figure 7,however, that the ratio div(B)/curl(B) is not very good in this region, while it is good everywhere else.

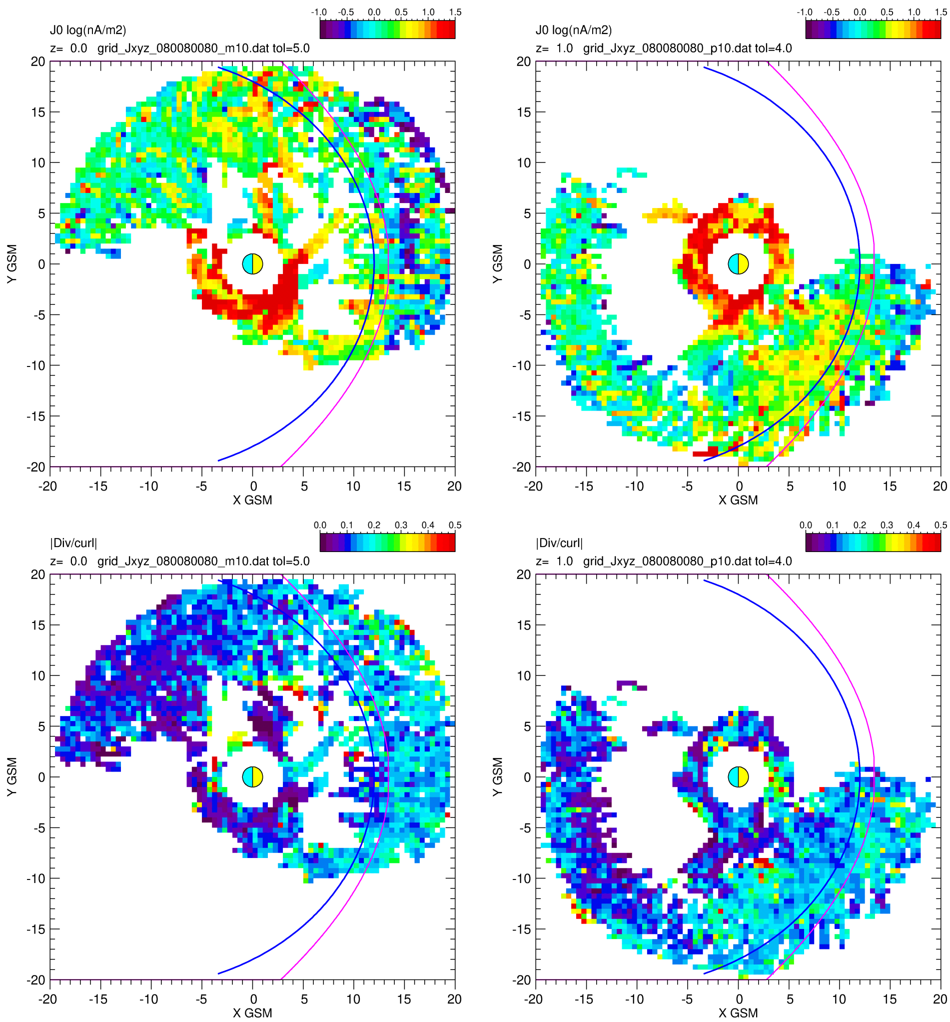

Figure 7. Top: current density magnitude in XY GSM plane, for dipole tilt angle θ = -10 (left) and +10 (right). Bottom: Div/Curl ratio.

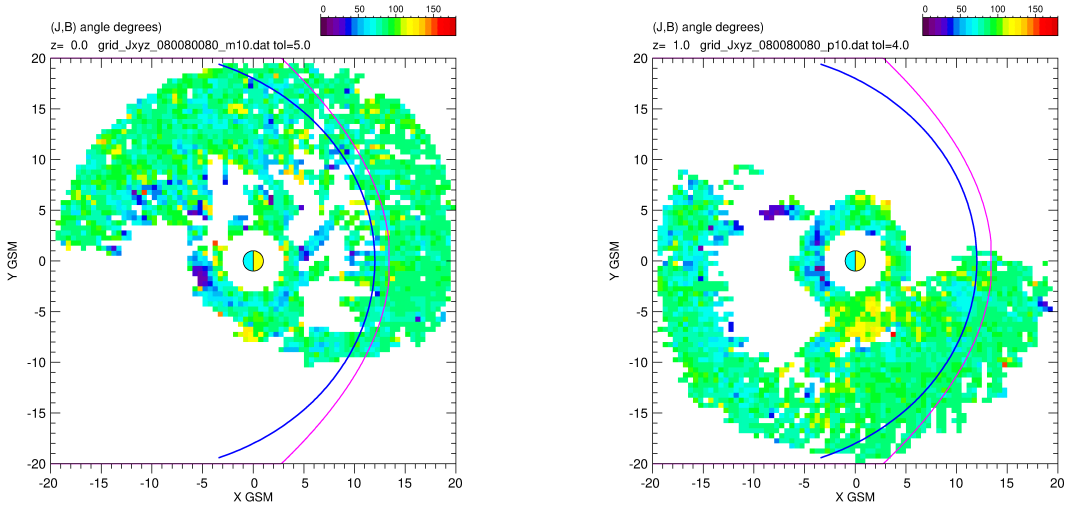

Figure 8. $(\vec{B}, \vec{J})$ angle in XY GSM plane, for dipole tilt angle θ = -10 (left) and +10 (right).

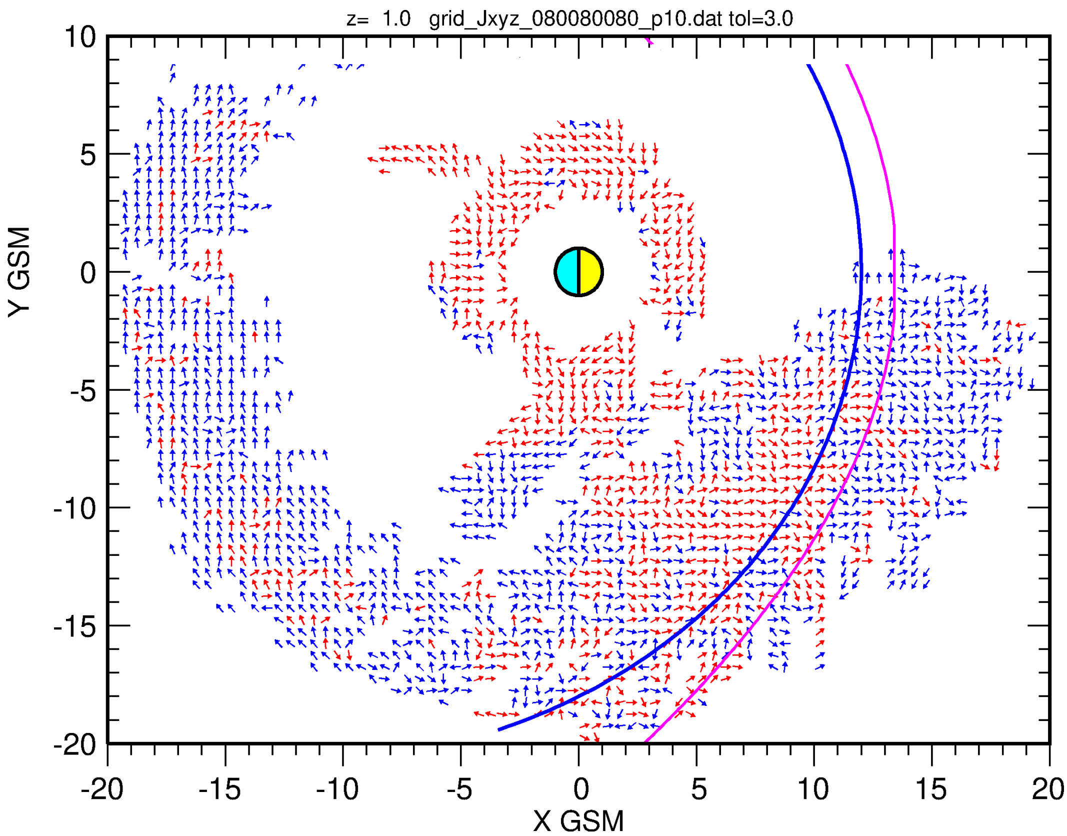

Figure 9. Direction of the current density in XY GSM plane for $\theta = 10$. Blue color correspond to intensity $< 1nA/m^2$, red for intensity $> 1nA/m^2$

5 Other Uses of the 3D Magnetic Field Grid

5.1 Limit of the closed field lines

The observation of the direction of $\vec{B}$ in the meridian and equatorial planes, for a fixed value of the dipole tilt angle, and for values averaged over twenty years, shows a very good organization of the field inside the magnetosphere. After the bow shock, the direction of the field becomes more disorganized, as expected. Hence, we propose to use these field maps to define the limit of closed field lines, essentially on the day side, where we have enough data. We are not using this limit to define the magnetopause, but it is useful as a point of interest to have a geometric reference for the plots. For the meridian plane, this limit is approximately fitted by half an ellipse, with major axis along Z and minor axis along X. The earth is taken as a focus of the ellipse, and we set two points of the ellipse as (X,Z)=(12,0) and (0,18). So the ellipse equation is $r(\theta) = p/(1+e\cos\theta)$ with $p = 18$ and $e = 0.5$.

This very simple shape and applies quite well to the average experimental data. We have verified that it also provides good results when the dipole tilt angle changes, up to plus or minus 30 degrees. This limit therefore can simply show the boundary between field lines having a defined geometry (closed field lines) and the part of space where they appear to be disorganized.A similar graph was made in the equatorial plane, with same parameters.

5.2 Spatial interpolation in the 3D grid

We therefore have the average values of the magnetic field in a 3-D grid of about 40 R_E with a resolution of 0.25 to $1R_E$ ($\sim$ 1000 to 6000 km). Of course, the higher the resolution is, the more empty the cells will be. However, from the files defined in section 2, we can create a grid of arbitrary resolution, depending on what we want to do. With this data grid, we can perform a 3-D interpollation in order to obtain a field value at any point in space. To proceed with this interpolation, we collect all the points in the grid inside a sphere of radius R_{max}, centered on the given point, and we carry out a weighted average of all the points with a Franke-Little weighting (Franke, 1982). Each point on the grid is at a distance :d_i from the requested point, where its corresponding weight is $W_i = max(1. - d_i/R_{max}, 0.)$. This means that any point beyond R_{max} will have zero weight.We have chosen this interpolation method for its simplicity and efficiency, with regard to the 4 million points to be processed for each grid. Thus, we can calculate the field at any point in space, and therefore apply the TRACE ray tracing subroutine of GEOPACK software (Tsyganenko, 2008), slightly modified to introduce the data produced from the 3D grid. Starting from a point in the space of the grid, we thus can calculate all the points of a magnetic field line.

5.2.1 Field Line in Meridian Plane

Figure 10 shows an example of ray tracing in the meridian plane. Of course, the lines are not complete, because the grid has a lot of empty cells, but we still get an overview of the mean field lines inside the magnetosphere. It should be noted that the greater the resolution of the grid, the more precise the interpolation will be, but also the longer will be the calculation time to obtain a field line. It would of course be preferable to interpolate directly from the initial point cloud instead of using the averaged point grid, but this creates too large a number (more than 600 million points) and makes this operation impossible on a small computer. A simple grid of 0.25 R_E resolution already contains 4 million points.

It is unfortunate that the zones of the northern cusp are not better defined, because of the empty cells, but nevertheless the general appearance of the field lines obtained is quite plausible. Figure 11 shows two other examples of field line tracing in the meridian plane, for dipole tilt angle = -20 (left) and +20 (right). For $\theta = -20$, the data grid does not contains many points, but enough to show the limit of the closed field lines, and the south cusp. For $\theta = +20$, the two cusps are visible.

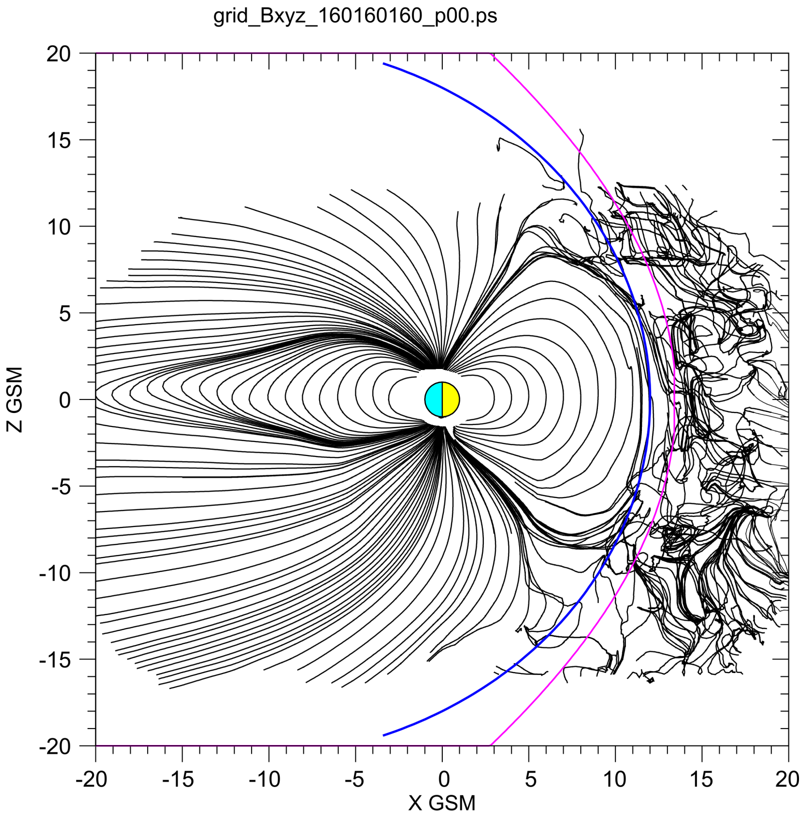

Figure 10. Field line tracing from spatial interpolation of B data grid, for $\theta = 0$

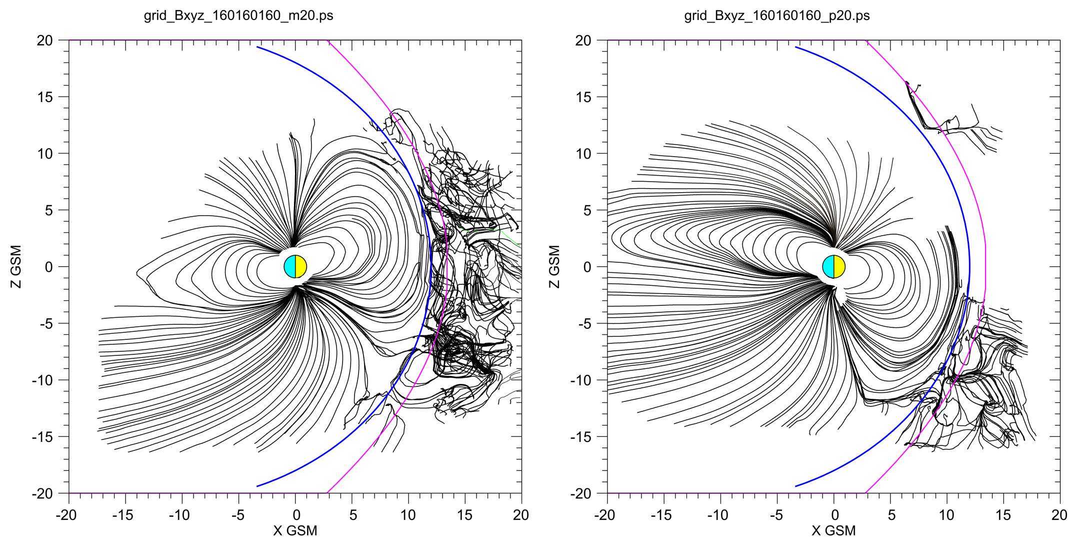

Figure 11. Same as Fig. 10 but for $\theta = -20$ (left) and $\theta = +20$ (right)

5.2.2 Field Line Near the Cusps

To visualize the field lines near the cusps, we place ourselves in a plane perpendicular to the mean cusp direction determined from figure 10, and at a distance of 4 and 10.5 R_E for the northern cusp, and at 5 and 11. R_E for the south cusp . The center of this Y-M system is assumed to be the center of the cusp. In this plane, we start the field lines computation from a series of points following a circle of radius of 2.5 R_E. The field lines are calculated in both directions, parallel and anti-parallel to $\vec{B}$.

The results are shown in Figures 12 and 13 for Northern and South cusps, with $\theta = 0$. The cone shape of the cusps is easily recognizable, although one more time nor the IMF or solar wind effects are taken into account.

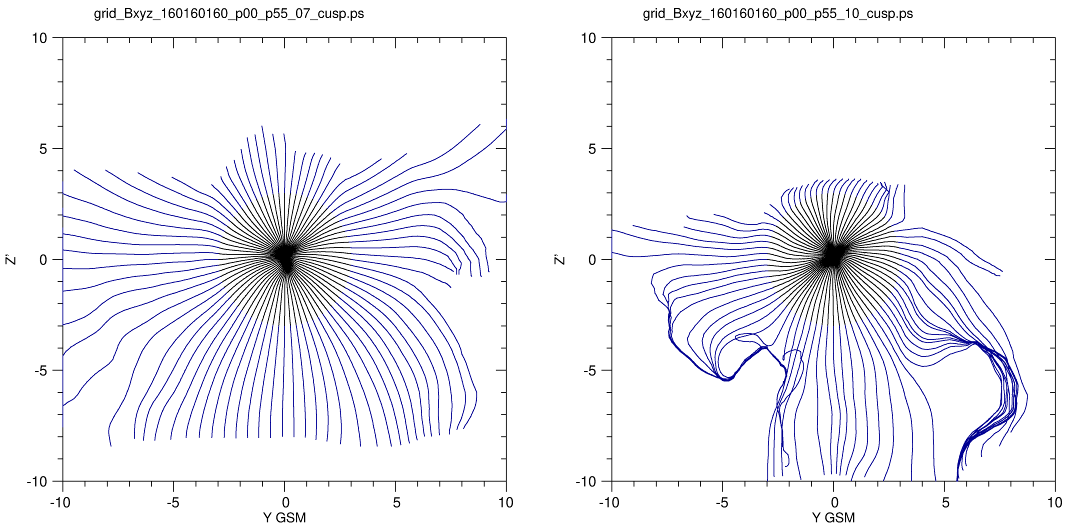

Figure 12. Field Line Tracing near the northern cusp for $\theta = 0$ and two values of the distance. Left: 7 R_E. Right:10. R_E .

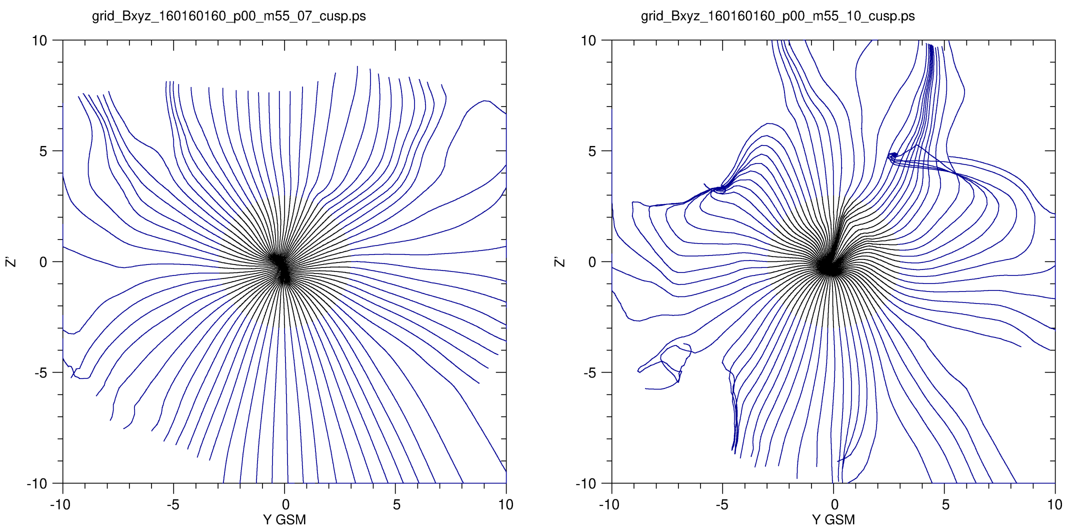

Figure 13. Field Line Tracing near the south cusp for $\theta = 0$ and two values of the distance. Left: 7 R_E. Right:10. R_E .

6 Conclusions

The use of twenty years of data of the FGM magnetometer made it possible to observe the average behaviour of the magnetic field, according to the values of the dipole tilt angle. The creation of a magnetic field database where all $\vec{B}$ and $\vec{P}$ vectors of the 4 spacecraft are time aligned made it possible to calculate curl and div of $\vec{B}$ over the entire duration of the mission, and made it possible to produce current density maps, in addition to those of the magnetic field. The validity of the estimate of this current density has been discussed. Note that the small-scale MMS configurations access a different plasma scales and allow comparison to plasma currents(Dunlop et al., 2018) which may be improve the validity of the estimate of $\vec{J}$.

A field average 3-D data grid was calculated for $\vec{B}$ and $\vec{J}$ and can be used for other studies. The possibility of adding data from other missions (THEMIS, MMS) to this grid would make it possible to obtain better spatial coverage, and therefore maps of direction and intensity more extensive in space, notably on the night side. This addition would also make it possible to fill a lot of empty cells in the grid, and to obtain more precise field line maps. Other indicators in addition to the dipole tilt angle could and should be added (magnetic indices, solar wind parameters). In future work it would be interesting to compare the B field maps with the Magnetic field Rotation Analysis method (MRA) developed by Shen et al. (2007), and comparisons to MHD models.

All the databases set up to carry out this work, as well as the reading and calculation codes (f90), can be made available to any interested person.

Acknowledgments

The authors are deeply grateful to the entire FGM team, past and present, for their ongoing efforts over more than 20 years to building a magnificent collection of magnetic field data over all these years. This work is supported by STFC in-house research grant ST/M001083/1, NSFC grants 41821003 and 41874193. Thanks to Philippe Escoubet for reading the manuscript and making useful comments and suggestions.

It is also thanks to the efforts of ESA's Cluster Science Archive (Laakso et al., 2010) that these data are now public (see `https://www.cosmos.esa.int/web/csa/access`), and their ease of access and download is remarkable and commendable .

References

Allen, A., Schwartz, S., Harvey, C., Perry, C., Huc, C., & Robert, P. (2004, apr 16). *Csds archive task group, "cluster exchange format, data file syntax", ds-qmw-tn-0010,issue 2 rev. 0, issue 2 rev. 0* (Tech. Rep.). Paris, France: ESA.

Balogh, A., Cowley, S. H., Dunlop, M., Southwood, D., Thomlinson, J., Glassmeier, K.-H., ... Tsurutani, B. (1993). The Cluster Magnetic Field Investigation: Scientific Objectives and Instrumentation. In R. Schmidt (Ed.), *Cluster: Mission, Payload and Supporting Activities* (p. 95-114). Paris, France: European Space Agency.

Balogh, A., Dunlop, M., Cowley, S. H., Southwood, D., Thomlinson, J., Glassmeier, K.-H., ... Kivelson, M. (1997). The Cluster magnetic field investigation. *Space Science Reviews*, *79*, 65-91.

Chanteur, G. (1998, July). Spatial interpolation fo four spacecraft: Theory. In G. Paschman & P. Daly (Eds.), *Analysis Methods for Multi-Spacecraft Data* (p. 349-369). European Space Agency.

Chanteur, G., & Harvey, C. (1998, July). Spatial interpolation fo four spacecraft: Application to magnetic gradients. In G. Paschman & P. Daly (Eds.), *Analysis Methods for Multi-Spacecraft Data* (p. 371-393). European Space Agency.

Chanteur, G., & Mottez, F. (1993). Geometrical tools for Cluster data analysis. In *Proc. international conf. "spatio-temporal analysis for resolving plasma turbulence (start)", aussois, 31 jan. 31–5 feb. 1993* (p. 341-344). Paris, France: European Space Agency.

Dunlop, M., Balogh, A., Southwood, D., Elphic, R. C., Glassmeier, K.-H., & Neubauer, F. M. (1990, May). Configurational sensitivity of multipoint magnetic field measurements. In E. Rolfe (Ed.), *Proceedings of the international workshop on "space plasma physics investigations by cluster and regatta", graz, feb. 20–22,1990* (p. 20-22). Paris, France: European Space Agency.

Dunlop, M., Southwood, D., Glassmeier, K.-H., & Neubauer, F. (1988). Analysis of multipoint magnetometer data. *aisr*, *8*, (9)273-(9)277.

Dunlop, M. W., Balogh, A., Glassmeier, K.-H., & Robert, P. (2002). Four-point cluster application of magnetic field analysis tools: The curlometer. *Journal of Geophysical Research: Space Physics*, *107*(A11), SMP 23-1-SMP 23-14. Retrieved from `https://agupubs.onlinelibrary.wiley.com/doi/abs/10.1029/2001JA005088` doi: https://doi.org/10.1029/2001JA005088

Dunlop, M. W., & Eastwood, J. P. (2008, January). The Curlometer and Other Gradient Based Methods. *ISSI Scientific Reports Series*, *8*, 17-26.

Dunlop, M. W., Haaland, S., Dong, X.-C., Middleton, H. R., Escoubet, C. P., Yang, Y.-Y., ... Russell, C. T. (2018). Multipoint analysis of electric currents in geospace using the curlometer technique. In *Electric currents in geospace and beyond* (p. 67-80). American Geophysical Union (AGU). Retrieved from `https://agupubs.onlinelibrary.wiley.com/doi/abs/10.1002/9781119324522.ch4` doi: https://doi.org/10.1002/9781119324522.ch4

Dunlop, M. W., Yang, J.-Y., Yang, Y.-Y., Lühr, H., & Cao, J.-B. (2020). Multi-spacecraft current estimates at swarm. In M. W. Dunlop & H. Lühr (Eds.), *Ionospheric multi-spacecraft analysis tools: Approaches for deriving ionospheric parameters* (pp. 83–116). Cham: Springer International Publishing. Retrieved from `https://doi.org/10.1007/978-3-030-26732-2_5` doi: 10.1007/978-3-030-26732-2_5

Franke, R. (1982). Scattered data interpolation: Tests of some methods. *Mathematics of Computation*, *38*, 181–200. doi: 10.2307/2007474

Khurana, K., Kepko, E., Kivelson, M., & Elphic, R. (1996). Accurate determination of magnetic field gradients from four point vector measurements: Ii. use of natural constraints on vector data obtained from four spinning spacecraft. *IEEE Trans. Magn.*, *32*, 5193.

Laakso, H., Perry, C., McCaffrey, S., Herment, D., Allen, A. J., Harvey, C. C., ... Turner, R. (2010, January). Cluster Active Archive: Overview. *Astrophysics and Space Science Proceedings*, *11*, 3-37. doi: 10.1007/978-90-481-3499-1_1

Robert, P., Dunlop, M., Roux, A., & Chanteur, G. (1998, July). Accuraccy of current density determination. In G. Paschman & P. Daly (Eds.), *Analysis Methods for Multi-Spacecraft Data* (p. 395-418). European Space Agency.

Robert, P., & Roux, A. (1990, may). Accuracy of the estimate of J via multipoint measurements. In E. Rolfe (Ed.), *Proceedings of the international workshop on "space plasma physics investigations by cluster and regatta", graz, feb. 20–22,1990* (p. 29-35). Paris, France: European Space Agency.

Robert, P., & Roux, A. (1993). Influence of the shape of the tetrahedron on the accuracy of the estimation of the current density. In *Proc. international conf. "spatio-temporal analysis for resolving plasma turbulence (start)", aussois, 31 jan. 31–5 feb. 1993* (p. 289-293). Paris, France: European Space Agency.

Robert, P., Roux, A., & Chanteur, G. (1995, July). Accuracy of the determination of the current density via four satellites. In *Abstracts.* Boulder, Colorado. (Presentation GAB51H-06)

Robert, P., Roux, A., & Coeur-Joly, O. (1995, June). Validity of the estimate of the current density along Cluster orbit with simulated magnetic data. In *Proceed-*

ings of cluster workshops, braunschweig, 28–30 sep. 1994, toulouse, 16–17 nov. 1994 (p. 229-233). Paris, France: European Space Agency.

Robert, P., Roux, A., Harvey, C., Dunlop, M., Daly, P., & Glassmeier, K.-H. (1998, July). Tetrahedron geometric factors. In G. Paschman & P. Daly (Eds.), *Analysis Methods for Multi-Spacecraft Data* (p. 323-348). European Space Agency.

Rodriguez-Canabal, J., Warhaut, M., Schmidt, R., & Bello-Mora, M. (1993, March). The Cluster orbit and mission scenario. In W. R. Burke (Ed.), *Cluster: Mission, payload and supporting activities* (Vol. 1159, p. 259).

Shen, C., Li, X., Dunlop, M., Shi, Q. Q., Liu, Z. X., Lucek, E., & Chen, Z. Q. (2007). Magnetic field rotation analysis and the applications. *Journal of Geophysical Research: Space Physics*, *112*(A6). Retrieved from `https://agupubs.onlinelibrary.wiley.com/doi/abs/10.1029/2005JA011584` doi: https://doi.org/10.1029/2005JA011584

Thébault, E., Finlay, C. C., Beggan, C. D., Alken, P., Aubert, J., Barrois, O., ... Zvereva, T. (2015, May 27). International geomagnetic reference field: the 12th generation. *Earth, Planets and Space*, *67*(1), 79. Retrieved from `https://doi.org/10.1186/s40623-015-0228-9` doi: 10.1186/s40623-015-0228-9

Tsyganenko, N. A. (2008). *Geopack: A set of fortran subroutines for computations of the geomagnetic field in the earth's magnetosphere* (Tech. Rep.). Retrieved from `http://geo.phys.spbu.ru/~tsyganenko/Geopack-2008.html`

Vallat, C., Dandouras, I., Dunlop, M., Balogh, A., Lucek, E., Parks, G. K., ... Rème, H. (2005). First current density measurements in the ring current region using simultaneous multi-spacecraft cluster-fgm data. *Annales Geophysicae*, *23*(5), 1849–1865. Retrieved from `https://angeo.copernicus.org/articles/23/1849/2005/` doi: 10.5194/angeo-23-1849-2005

Yang, J., Toffoletto, F. R., Wolf, R. A., Sazykin, S., Ontiveros, P. A., & Weygand, J. M. (2012). Large-scale current systems and ground magnetic disturbance during deep substorm injections. *Journal of Geophysical Research: Space Physics*, *117*(A4). Retrieved from `https://agupubs.onlinelibrary.wiley.com/doi/abs/10.1029/2011JA017415` doi: https://doi.org/10.1029/2011JA017415

Zhang, Q.-H., Dunlop, M. W., Lockwood, M., Holme, R., Kamide, Y., Baumjohann, W., ... Liu, S.-L. (2011). The distribution of the ring current: Cluster observations. *Annales Geophysicae*, *29*(9), 1655–1662. Retrieved from `https://angeo.copernicus.org/articles/29/1655/2011/` doi: 10.5194/angeo-29-1655-2011